RSC Advances

PAPER

View Article Online
View Journal | View Issue

Cite this: *RSC Adv.*, 2020, **10**, 39226

Global accurate diabatic potential surfaces for the reaction H + Li_2

Ruilin Yin,†[a] Nan Gao,†[b] Jing Cao,[a] Yanchun Li,[a] Dequan Wang *[a] and Xuri Huang[a]

Received 2nd July 2020
Accepted 21st September 2020

DOI: 10.1039/d0ra05777k

rsc.li/rsc-advances

The adiabatic potential energies for the lowest three states of a Li_2H system are calculated with a high level *ab initio* method (MCSCF/MRCI) with a large basis set (aV5Z). The accurate three dimensional B-spline fitting method is used to map the global adiabatic potential energy surfaces, using the existing adiabatic potential energies, for the lowest two adiabatic states of the title reaction system. The different vibrational states and corresponding energies are studied for the diatomic molecule of reactant and products. In order to clearly understand the nonadiabatic process, the avoided crossing area and conical intersection are carefully studied. For further study of the nonadiabatic dynamic reaction, the diabatic potential energy surfaces are deduced in the present work.

1 Introduction

Scattering reactions play an important role in atomic and molecular collision dynamics. The collisions involving hydrogen atoms and lithium molecules play a central role in chemical physics because they can provide essential mechanistic information for understanding lithium chemistry, which was very important in early cosmic evolution.[1–8] These reactions are significant in stellar evolution and galactic lithium production, as are LiH molecule formation and depletion processes.[9,10] In addition to hydrogen, lithium is a key element in cosmology, galactic evolution and stellar models.[9] The title reaction may have created the first condensed structure in the early universe,[11,12] and the reaction can also show lithium neutron shielding and hydrogen storage processes.[13,14] As the simplest mixed cluster, the Li_2H trimer has become a focus of research efforts both experimentally[15–17] and theoretically.[18–33]

Wu and Ihle[15] proved the existence of stable Li_2H first in 1977, using mass spectroscopy measurements of dilute solutions of hydrogen in liquid lithium. The atomization energy value of 89.7 ± 5.0 kcal mol^{-1} was found in their work. The second experiment was reported by Vezin *et al.*[16] in 1993. The experimental optical spectrum, the geometries in ground and excited states, of the title system were expressed. The third experiment for Li_2H was by Antoine *et al.*,[17] and in Antoine's work, the ground state $^2A_1$ and two excited states $^2B_1$ and $^2B_2$, were observed.

A large number of theoretical studies were essential in the identification and understanding of the Li_2H system. The investigation of an accurate electronic potential energy surface (PES) is the first essential ingredient. Up to now, there are six PESs that can be used to introduce the Li_2H system. Siegbahn and Schaefer[19] got the first PES of Li_2H with a self-consistent-field wave function and full configuration interaction method in 1975. Followed by Kim and Herschbach,[21] who constructed a new PES with a well depth of 3.812 eV. In 2010, Maniero *et al.*[25] obtained PES of the ground state Li_2H with full configuration interactions using 394 energy points using a 6-311G(2df,2pd) basis set, which indicated that the H + $Li_2(X^1\Sigma_g^+)$ → Li + LiH($X^1\Sigma$+) is a barrierless exothermic reaction, and the reaction will release 1.474 eV energy. In 2011, Skomorowski *et al.*[26] calculated the IEA between the lithium atom and the lithium hydride molecule using Jacobi coordinate with CCSD(T) method, and a conical intersection was reported. More recently, Song *et al.*[28] calculated 3726 *ab initio* potential energies using a CASSCF/MRCI method to map a new global adiabatic PES of the electronic ground-state of Li_2H. In 2017, Yuan and co-authors[30] constructed an accurate PES over a large configuration space with 29 842 energy points, which were calculated at the CASSCF/MRCI-F12 level using a CC-pVTZ basis set. Subsequently, the reaction dynamic calculations for the title system were performed based on these PESs.

The H + Li_2 reaction is exothermic, and there are relative deep potential wells on the reaction path, furthermore, the geometry of the conical intersection is near the bottom of the potential wells which means that the transformation between the lowest two PES states is easy. Thus, the nonadiabatic interactions between the ground state and the excited states may play an important role. The diabatic potential energy

[a]*Institute of Theoretical Chemistry, Jilin University, Changchun, People's Republic of China. E-mail: dequan_wang@jlu.edu.cn*

[b]*Department of Thoracic Surgery, China-Japan Union Hospital of Jilin University, Changchun, People's Republic of China*

† These authors contributed equally to the work.

surface can be used to express this electron transform progress.

Up to now, no accurate diabatic PES exists for the nonadiabatic dynamic study of the H + Li_2 reaction. The main aim of this work is to perform a globally accurate diabatic PES, including the lowest two adiabatic PESs of Li_2H, using the MCSCF/MRCI level. First, the lowest three adiabatic PESs are mapped. The spectrum for LiH and Li_2 are studied to confirm the accuracy of these adiabatic PESs. Second, the accurate mixing angle data, which can be used to transform the adiabatic PES to diabatic PES, are calculated. Third, the avoided crossing point, which is between the lowest two adiabatic states, is accurately studied.

This paper is organized as follows: in the next section, the theory for mapping the adiabatic PESs and mixing angles is outlined. The features for adiabatic PESs, spectra, the avoided crossing point, mixing angles, and the diabatic PESs, will be presented and discussed in the third section. In the last section, a simple summary and conclusion will be provided.

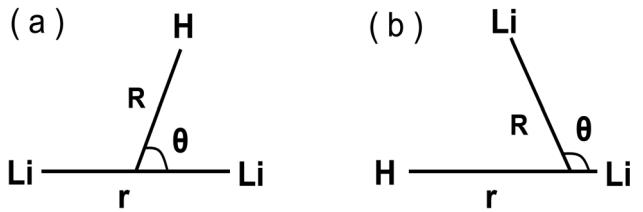

Fig. 1 Jacobi coordinates. (a) Reactant Jacobi coordinates, (b) product Jacobi coordinates.

2 Computational methods

2.1 *Ab initio* calculation

All *ab initio* calculations have been performed at the MCSCF/MRCI level with large basis sets (aV5Z)[34] using the MOLPRO 2012 package[35] for the three lowest state adiabatic potential energies of the Li_2H system. The symmetry of the title system is fixed in the C_s point group, in total, 7 electrons are involved in 2 closed-shell orbitals ($2A' + 0A''$). A total of 13 ($10A' + 3A''$) active orbitals are considered in the present work. And 319 ($192A' + 127A''$) external orbitals are used in this work. Thus the MCSCF function included 570 determinants and 1014 intermediate states for the triatomic molecule system. In the MRCI calculated progress, 2 orbitals ($2A' + 0A''$) are put into the core orbital, and 3 electrons are set in the valence space, the total number of contracted configurations is 705 202, which includes the number of internal configurations, single external configurations, and doubly external configurations – 420, 28 548, and 676 234, respectively. The energies of the lowest five states are considered as the reference energies to reduce the final three adiabatic potential energies.

There are several coordinate systems that can be used to describe the triatomic molecules. In these systems, Jacobi coordinates, which have been widely used in our former studies,[36–41] are the most popular ones to describe the three atoms scattering reaction, since it well expresses both the reactant part (H + Li_2) and product part (LiH + Li), which are shown in panel (a) and panel (b) in Fig. 1, respectively.

In this study, the potential energy points scanned are as follows: when r in the range 0.6 Å to 3.0 Å is calculated with a grid of 0.1 Å, when r is between 3.0 Å and 5.0 Å, the grid is 0.2

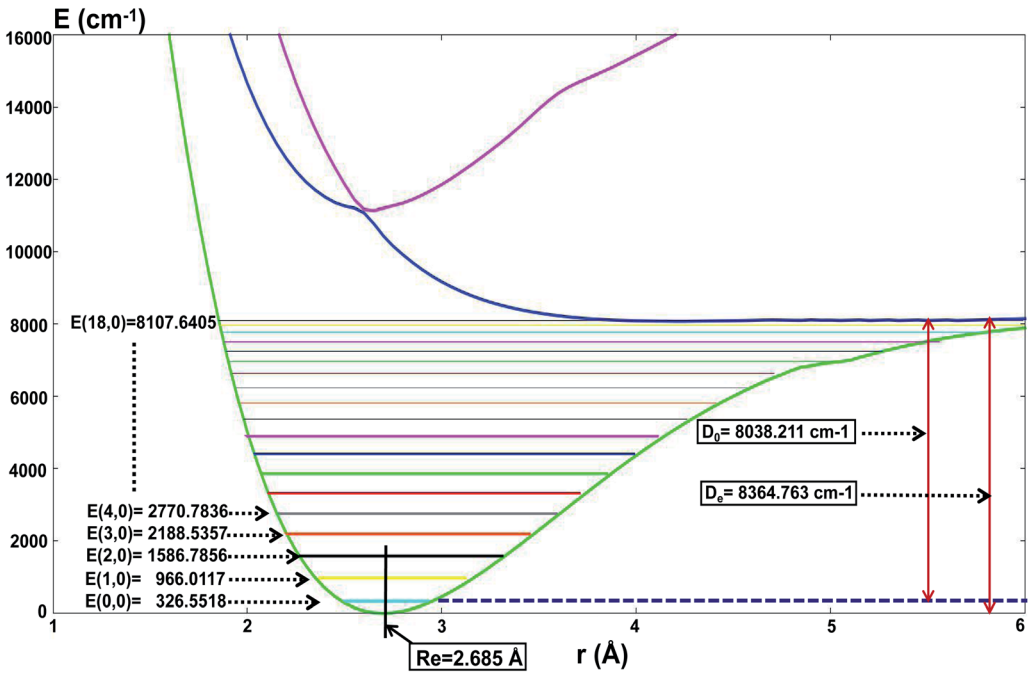

Fig. 2 The lowest three PESs (in cm^{-1}) for Li_2 as a function of distance r_{Li-Li} (in Å), and the different vibrational state energies $E(v,j = 0)$ (in cm^{-1}) of the ground state of Li_2.

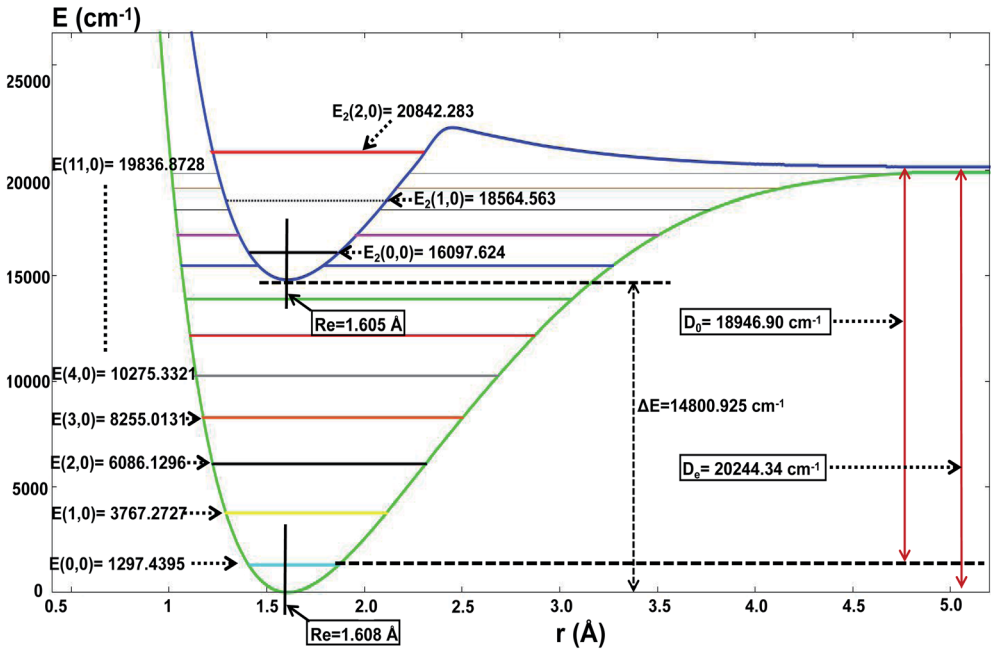

Fig. 3 The lowest two PESs (in cm^{-1}) for LiH as a function of distance r_{Li-H} (in Å), and the different vibrational state energies $E(v,j=0)$ (in cm^{-1}).

Å; for the R, when it is larger than 0.1 Å, and less than 3.0 Å, the scan grid is 0.1 Å, when 3.0 Å $\leq R \leq$ 7.0 Å the scan grid is 0.2 Å, and when R is in the range 7.0 Å to 11.8 Å, the grid is 0.4 Å; for the reactant region, the angles θ, with a grid of 10.0°, are scanned from 0.0° to 90.0°. In total 27 900 adiabatic potential energy points are mapped for each state in this reactant area; for the product region, the angles used are from 0.0° to 180.0° with the same scan grid, the total scan points are 46 170 for each state; thus 74 070 adiabatic potential energy points are used to produce the accurate adiabatic PESs for each state. In the whole scan range, a three dimension B-spline method[42,43] is used to interpolate the surfaces.

2.2 Internal energy calculations

The discrete eigenvalues and eigenfunctions of the related vibrational (v) and rotational (j) states for the internal energy $E_{v,j}$ can be determined with the one-dimensional Schrödinger equation. The Schrödinger equation is given as

$$-\frac{\hbar^2}{2\mu}\frac{d^2\Psi_{v,j}(r)}{dr^2} + V_j(r)\Psi_{v,j}(r) = E_{v,j}\Psi_{v,j}(r) \quad (1)$$

μ is the reduced mass of the LiH and Li_2, $V_j(r)$ contains the rotationless potential $V(r)$ and a centrifugal potential. The centrifugal term for LiH and Li_2, $V_j(r)$ has the form $[j(j+1)-\Omega]\frac{\hbar^2}{2\mu r^2}$, where Ω is the projection of the electronic angular momentum onto the internuclear axis (see Level 8.0, p.2 (ref. 44) and the PhD thesis of Wang[45]).

2.3 Mixing angle (α) calculations

For calculating the mixing angles between the lowest two adiabatic states, the third adiabatic state, which is not involved

Table 1 Fitted data for LiH, Li_2 and Li_2H

Species	Parameter	This work	Other work	Experimental
Li_2	R_e [Å]	2.685	2.687[a], 2.674[b], 2.703[g]	2.525[c]
	D_e [cm^{-1}]	8364.76	8371.04[a], 8533.46[b]	8471.72[c]
	D_0 [cm^{-1}]	8038.21	8197.18[a], 7307.38[a]	
LiH	R_e [Å]	1.608	1.587[a], 1.596[b] 1.622[g]	1.597[e]
	D_e [cm^{-1}]	20 244.34	20 342.60[d], 20 293.19[b]	20 287.70[e]
	D_0 [cm^{-1}]	18 946.90	19 629.10[d], 16 090.75[g]	19 589.80[e]
Li_2H	R_{H-Li} [Å]	1.723		
	Θ [°]	42.755	42.813[b]	42.708[b]
	E [kcal mol^{-1}]	82.295	86.900[f]	87.9 ± 3.0[f]

[a] Ref. 49. [b] Ref. 30. [c] Ref. 50. [d] Ref. 37. [e] Ref. 51. [f] Ref. 25. [g] Ref. 52.

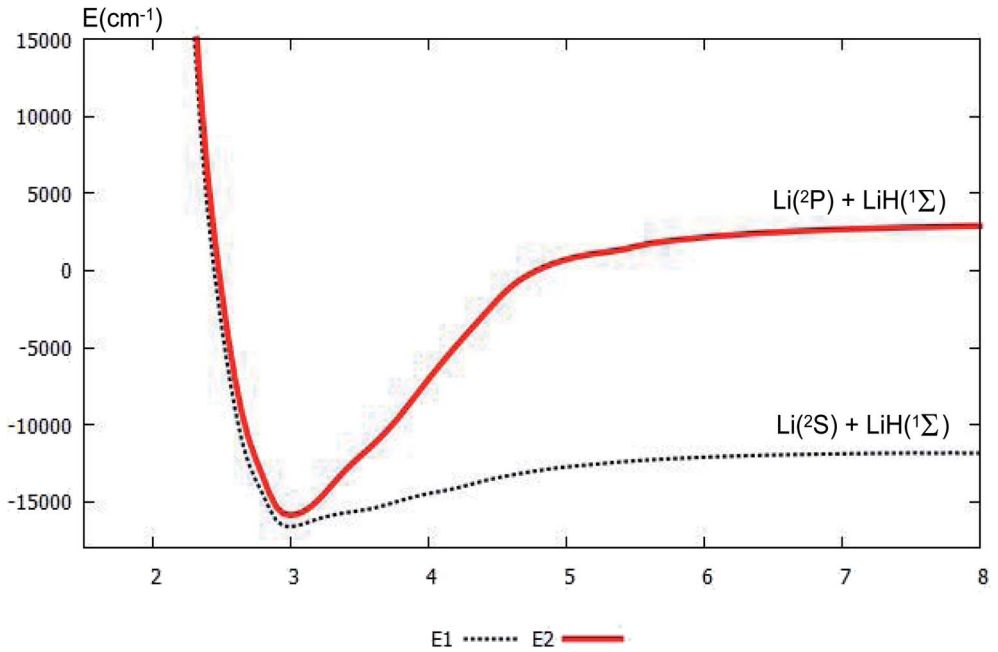

Fig. 4 The lowest two PESs (in cm^{-1}) for $Li(^2S/^2P) + LiH(^1\Sigma)$ with the function of R_{Li-LiH} (in Å), and distances $r_{Li-H} = 1.61$ Å at angle $\theta = 0.0°$ using product Jacobi coordinates.

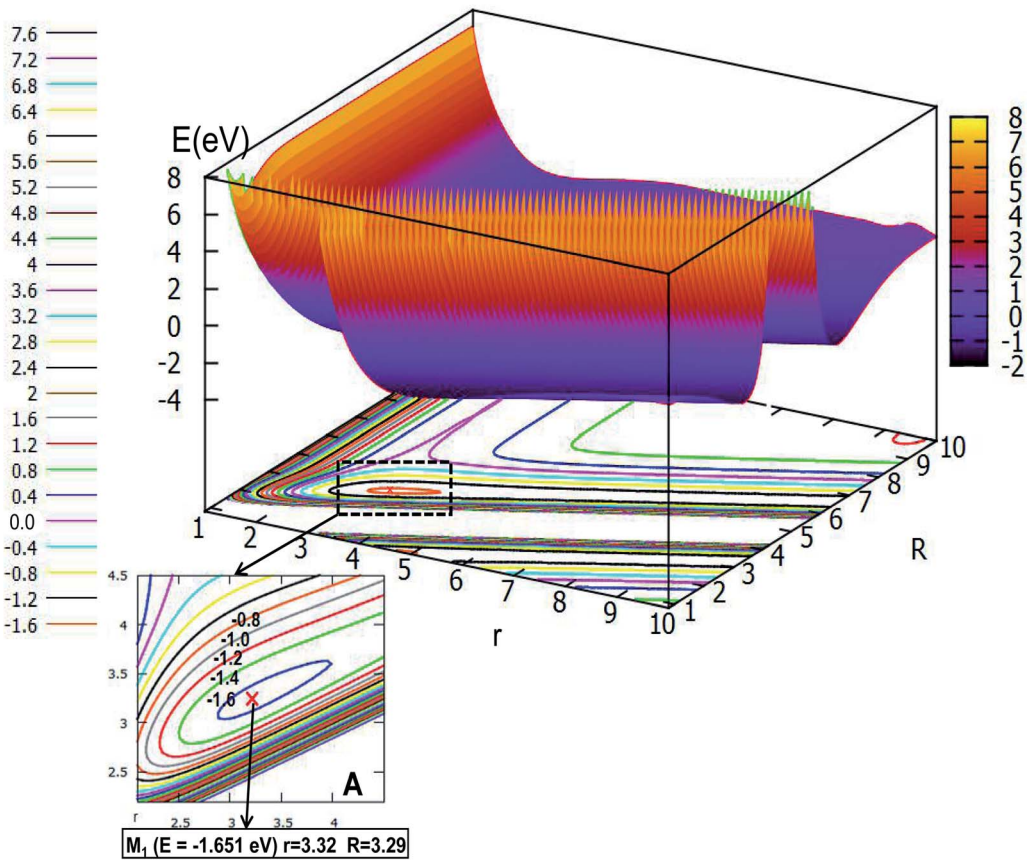

Fig. 5 The lowest potential energy surface (in eV) for Li_2H and its contour plot as a function of distances r and R (in Å) at angle $\theta = 0.0°$ in Jacobi coordinates.

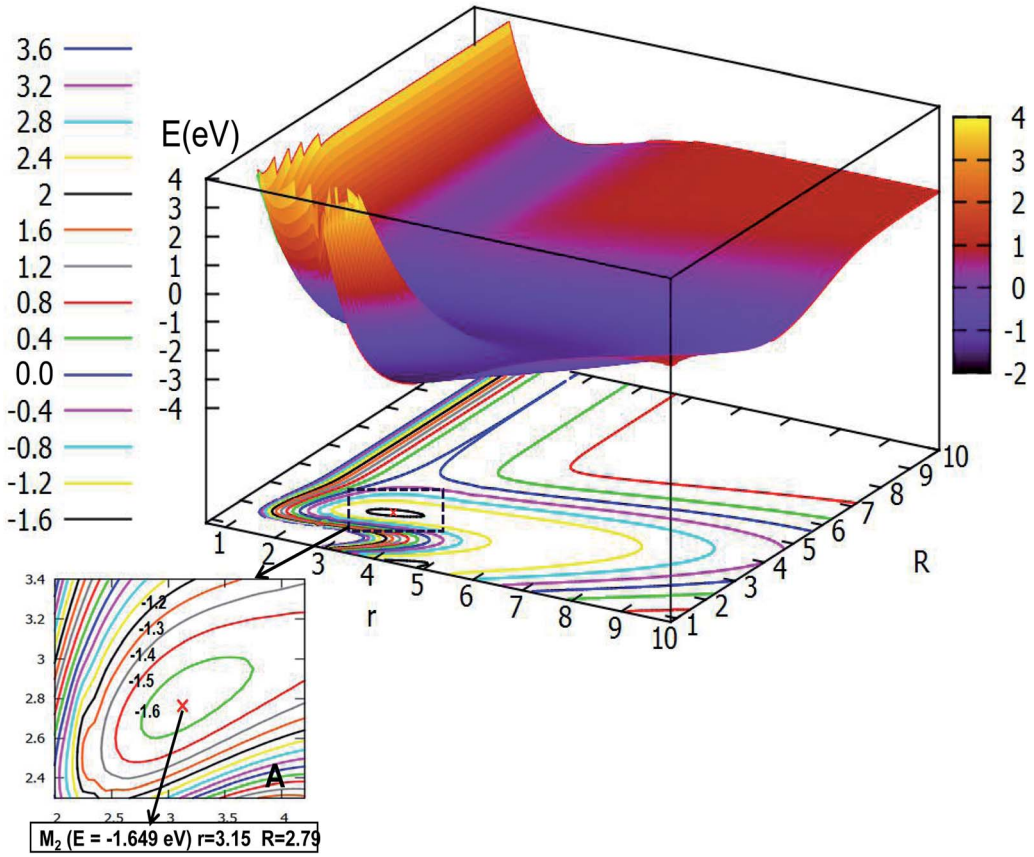

Fig. 6 The lowest potential energy surface (in eV) for Li_2H and its contour plot of the potential energy surface as a function of distances r and R (in Å) at angle $\theta = 30.0°$ in Jacobi coordinates.

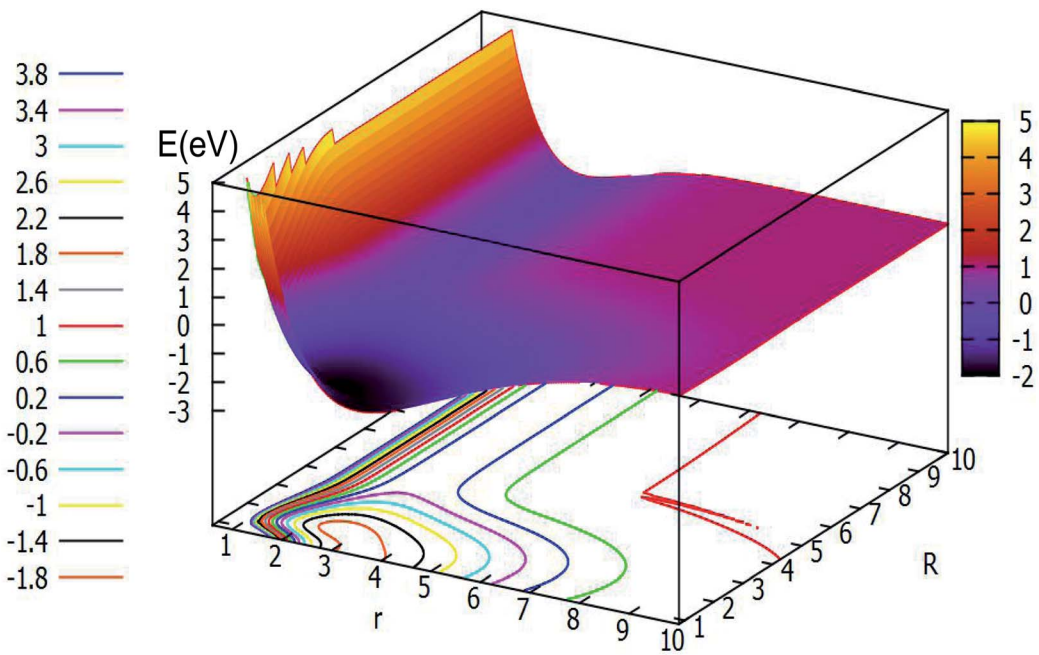

Fig. 7 The lowest potential energy surface (in eV) for Li_2H and its contour plot of the potential energy surface as a function of distances r and R (in Å) at angle $\theta = 60.0°$ in Jacobi coordinates.

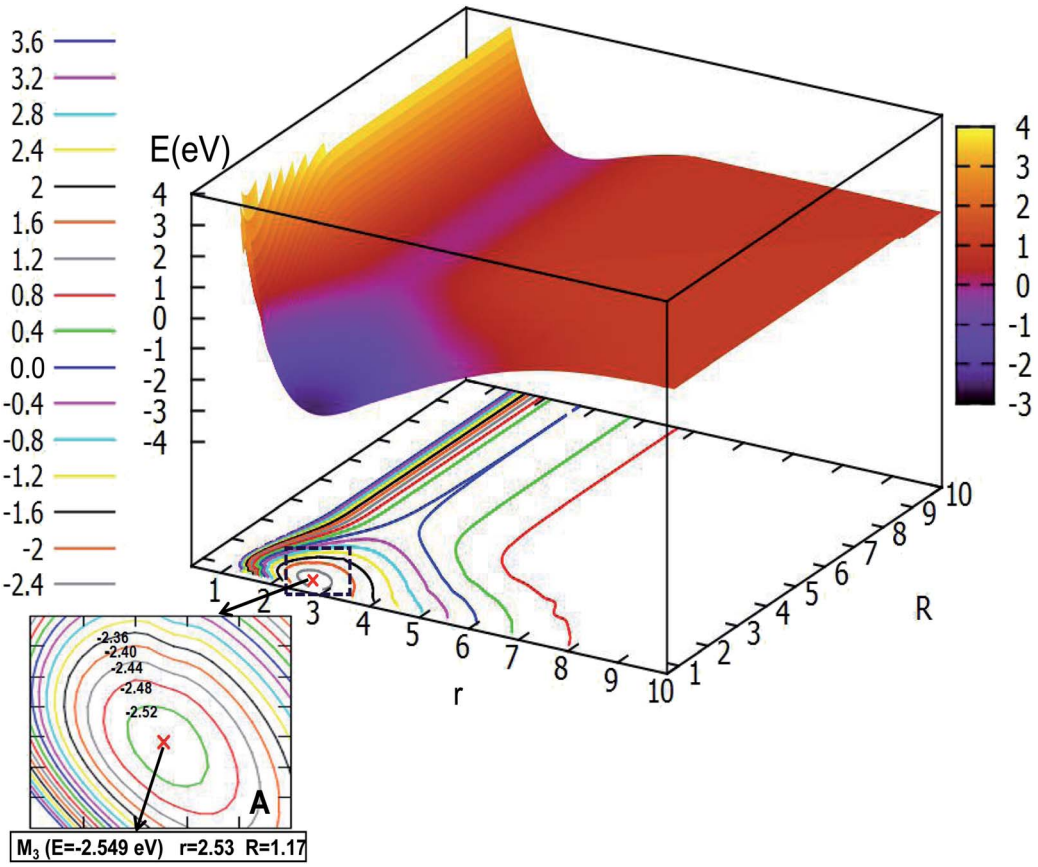

Fig. 8 The lowest potential energy surface (in eV) for Li_2H and its contour plot of the potential energy surface as a function of distances r and R (in Å) at angle $\theta = 90.0°$ in Jacobi coordinates. The minimum area is enlarged and plotted in the same figure.

in the coupling, is scanned, this method has been widely used in He and Han's work.[46,47] The wave functions are ψ_1^a, ψ_2^a, and ψ_3^a of the first three lowest states. The adiabatic wave function of the lowest two states can be expressed as:

$$\begin{pmatrix} \psi_1^a \\ \psi_2^a \end{pmatrix} = \begin{pmatrix} \cos\alpha & \sin\alpha \\ -\sin\alpha & \cos\alpha \end{pmatrix} \begin{pmatrix} \phi_1^d \\ \phi_2^d \end{pmatrix}. \quad (2)$$

By multiplying by $\langle\psi_3^a|\hat{P}_z|$ (here $\hat{P}_z$ is the z component of the dipole moment operator) on both sides of eqn (2), the following two equations can be deduced:

$$\langle\psi_3^a|\hat{P}_z|\psi_1^a\rangle = \cos\alpha\langle\psi_3^a|\hat{P}_z|\phi_1^d\rangle + \sin\alpha\langle\psi_3^a|\hat{P}_z|\phi_2^d\rangle \quad (3)$$

$$\langle\psi_3^a|\hat{P}_z|\psi_2^a\rangle = -\sin\alpha\langle\psi_3^a|\hat{P}_z|\phi_1^d\rangle + \cos\alpha\langle\psi_3^a|\hat{P}_z|\phi_2^d\rangle. \quad (4)$$

In eqn (3) and (4), $\langle\psi_3^a|\hat{P}_z|\phi_1^d\rangle = 0$ and $\langle\psi_3^a|\hat{P}_z|\phi_2^d\rangle = 1$ at the high symmetry geometries (C_{2v}, D_{2h}). In the present work, an approximation[48] is made for all C_s symmetry geometries, *i.e.* $\langle\psi_3^a|\hat{P}_z|\phi_1^d\rangle = 0$ and $\langle\psi_3^a|\hat{P}_z|\phi_2^d\rangle = 1$ for all possible structures. Thus, the mixing angle α can be calculated as

$$\alpha = \arctan\left(\frac{\langle\psi_3^a|\hat{P}_z|\psi_1^a\rangle}{\langle\psi_3^a|\hat{P}_z|\psi_2^a\rangle}\right). \quad (5)$$

2.4 Adiabatic-to-diabatic transformation

After obtaining the mixing angle, we can deduce the diabatic function ϕ_i^d with the adiabatic function using the following equation

$$\begin{pmatrix} \phi_1^d \\ \phi_2^d \end{pmatrix} = \begin{pmatrix} \cos\alpha & -\sin\alpha \\ \sin\alpha & \cos\alpha \end{pmatrix} \begin{pmatrix} \psi_1^a \\ \psi_2^a \end{pmatrix}. \quad (6)$$

Then the diabatic energies H_{ii}^d can be obtained as

$$H_{11}^d = (\cos\alpha)^2 E_1^a + (\sin\alpha)^2 E_2^a, \quad (7)$$

$$H_{22}^d = (\sin\alpha)^2 E_1^a + (\cos\alpha)^2 E_2^a, \quad (8)$$

$$H_{12}^d = H_{21}^d = \sin\alpha\cos\alpha(E_2^a - E_1^a). \quad (9)$$

3 Results and discussion

The lowest three adiabatic PESs of the title reaction system are mapped, and the lowest two diabatic PESs are transformed, in the present work. For a clearer understanding of the features of these PESs, the lowest state energy of H + Li_2 is shifted to 0.00 eV. The details of the feature of these PESs is expressed in the following part.

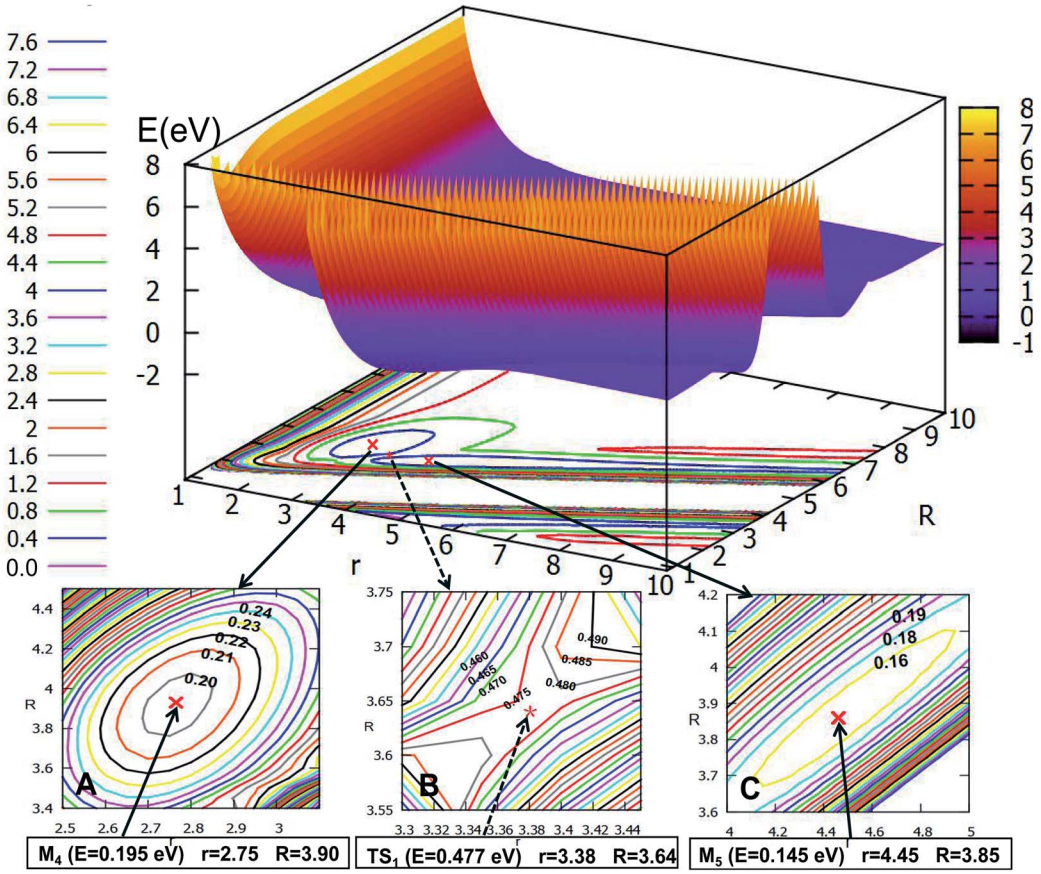

Fig. 9 PES for the first excited state of Li_2H and its contour plot as a function of distances r and R (in Å) at angle $\theta = 0.0°$ in Jacobi coordinates. (A) Enlarged plot of the linear reactant complex of Li–Li···H; (B) enlarged plot of the transition state transformed between (A and C); (C) enlarged plot of the linear product complex of Li···Li–H.

3.1 Features of one-dimensional (1D) diatomic adiabatic potential energy surfaces

For the present globally fitted PESs, one atom (Li or H) is fixed far away from the diatom molecule, and the 1D adiabatic PESs for Li_2 and LiH can be obtained as shown in Fig. 2 and 3. And the corresponding different level of vibrational and rotational energies (internal energies) for the ground state of Li_2 are deduced with the Level 8.0 program.[44] To obtain the Li_2 PESs, R is fixed at 11.0 Å and θ is fixed at 90° using the reactant coordinate. To obtain the ground and the first excited state PESs of LiH, we fixed $R = 11.0$ Å and $\theta = 90°$ with product coordinates. For ease of discussion of the PESs and the energies of different vibrational states, the energy of the equilibrium LiH molecule is shifted to 0.00 cm^{-1}. The detailed data of equilibrium bond distance (R_e) and dissociation energy (D_e) for Li_2 and LiH are shown in Table 1.

Fig. 2 shows that the equilibrium bond distance (R_e) is 2.685 Å for a Li_2 molecule. The corresponding dissociation energy (D_e) is 8364.76 cm^{-1}. These results are in good agreement with Jason's results[49] (2.687 Å and 8371.04 cm^{-1}). In total, 19 vibrational bound levels are found for the Li_2 molecule. The energy of the ground ro-vibrational state is $E(0,0) = 326.558$ cm^{-1} which is in good agreement with Angelo and Paulo's work[52] ($E(0,0) =$ 346.05 cm^{-1}). The energy of the highest vibrational state is $E(18,0) = 8107.64$ cm^{-1}.

From Fig. 2 one can see that there is no stable bond level for the first excited adiabatic state of Li_2. But there exist some stable bond levels for the second excited adiabatic state, which are not further studied in the present work.

Fig. 3 and Table 1 show the data for a LiH molecule. The detailed fitted data in the present work is as follows: for the ground state of LiH, there are 12 vibrational states; and the zero point energy is 1297.44 cm^{-1}, which approximates Angelo and Paulo's work[52] ($E(0,0) = 1363.05$ cm^{-1}); the dissociation energy is 18 946.90 cm^{-1}, which is in excellent agreement with the experiment result[51] (19 589.80 cm^{-1}); the equilibrium bond distance for LiH is 1.608 Å, which is nearly equal to the experiment result[51] (1.597 Å). For the first excited state of LiH, there are 3 vibrational states; the zero point energy of the excited state LiH is 16 097.62 cm^{-1}; the equilibrium bond distance is 1.605 Å; the lowest energy of the first excited state is 14 800.92 cm^{-1} higher than that of the ground state. When the two atoms separate from each other, the potential energy of these two states will degenerate to the same one.

Table 1 shows the data for the Li_2H molecule, the bond length of LiH is stretched from 1.608 Å to 1.723 Å, the angle

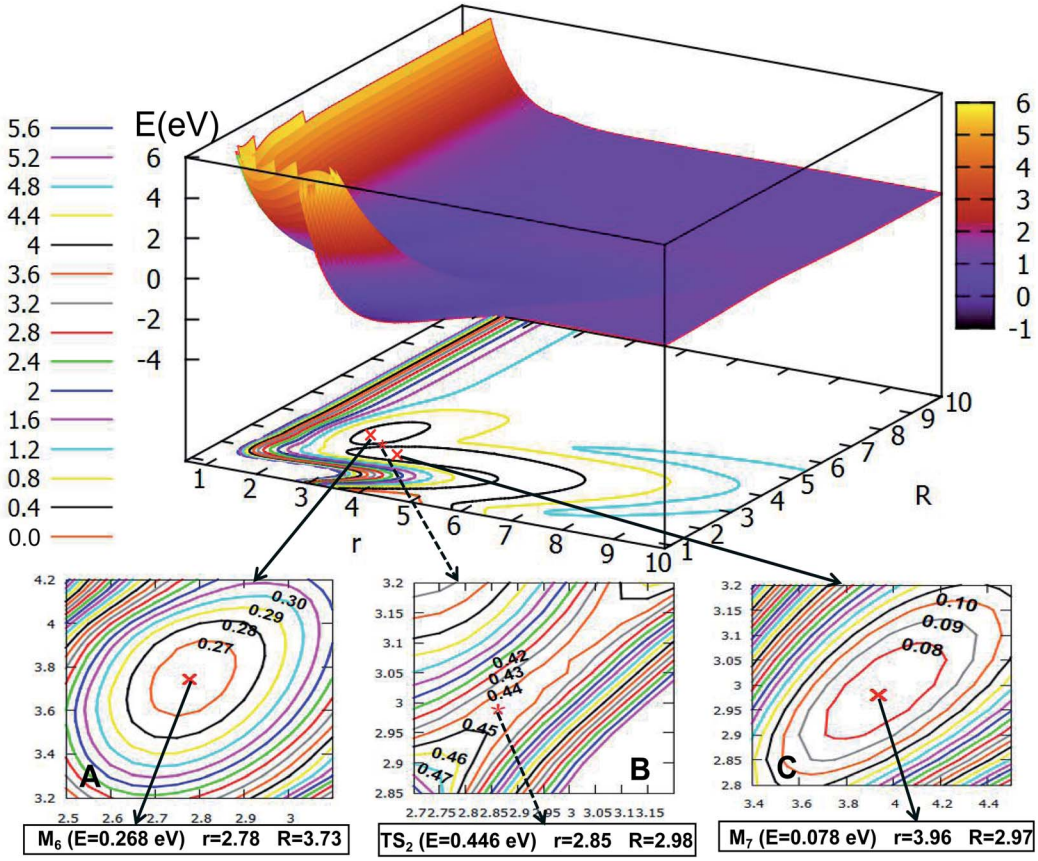

Fig. 10 The first excited state potential energy surface (in eV) for Li_2H and its contour plot as a function of distances r and R (in Å) at angle $\theta = 30.0°$ in Jacobi coordinates. (A) Enlarged plot of the minimum part M_6; (B) enlarged plot near the transition state part, TS_2; (C) enlarged plot of the minimum part of M_7.

between these two bonds is 42.8°, which is in good agreement with the experimental conclusion.[25,30]

For clear understanding of the adiabatic PESs of the products part, the PESs of $Li(^2S/^2P) + LiH(^1\Sigma)$ are plotted in Fig. 4. For this figure, the bond distance of the diatomic molecule LiH is fixed at 1.61 Å, and the angle is fixed at 0.0°. Fig. 4 shows that the minimum for this system is R nearly equal 3.0 Å. When R is less than 3.0 Å, the energies for the ground state and the first excited state are nearly the same. When the R is larger than 3.0 Å, the curves of the ground state and the first excited state separate; and when the Li atom separates from the LiH molecule, the energy differences between the two states equal the different energy of $Li(^2S)$ and $Li(^2P)$, this difference in energy is 14 854 cm^{-1}, which agrees well with our former work, 14 803 cm^{-1} (ref. 37), and experimental work, 14 904 cm^{-1}.[53]

3.2 Two-dimensional (2D) adiabatic PESs

3.2.1 2D adiabatic PESs of the ground state. In order to better describe the reaction process, we introduce the image of 3D PESs for analysis. The following figures (Fig. 5–12) represent PESs at different angles (including 0°, 30°, 60°, and 90°) of the ground state and the first excited state. In each figure, the upper part is the 2D PES, and the lower part is the contour plot of the 2D PES, with the 0.2 eV contour interval, some important parts are enlarged and plotted in the same figure. In these figures, the x-coordinate is r (in Å), the y-coordinate is R (in Å) and the z-coordinate is E (in eV).

Fig. 5 shows the lowest PES for Li_2H and its contour plot as a function of distances r and R at angle $\theta = 0.0°$ in Jacobi coordinates. It is not hard to see from the picture that there is a minimum whose energy is −1.651 eV, and the R value is 3.29 Å, while the r value is 3.32 Å. This minimum is a linear complex of Li···LiH. With increasing R value, the amplitude of the PES becomes flatter and flatter until there are nearly no changes, which means that as the distances r and R become longer, the interaction between these three atoms decreases to zero, thus, the three atoms in the Li_2H system separate each other. On the contrary, as the r value becomes small, when the R value is between 2.0 Å and 5.0 Å, then the geometry of the minimum is formed; if the R value is less than 2.0 Å, there is higher energy.

Fig. 6 expresses the PES and the corresponding contour plot in angle $\theta = 30.0°$. Comparing the previous pictures, the initial configuration changes from the liner geometry to a certain angle of inclination, that is why the two pictures of products export differently. From the image we find that the reaction entrance is smooth when the r value is small and the R value is big, until the value of R decreases to 4.0 Å, then the PES gradually tends to form the lowest point configuration, at which the

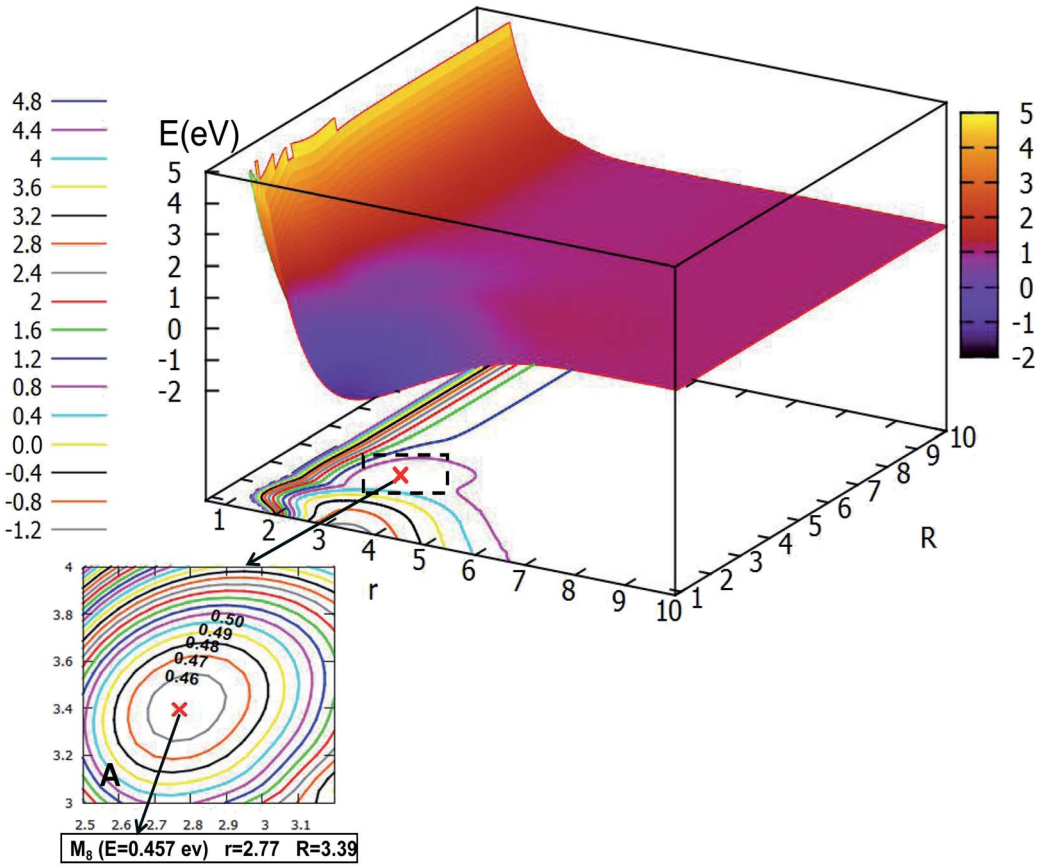

Fig. 11 The first excited state potential energy surface (in eV) for Li_2H and its contour plot as a function of distances r and R (in Å) at angle $\theta = 60.0^\circ$ in Jacobi coordinates. (A) Enlarged plot of the minimum part.

r value is 3.15 Å and the R value is 2.79 Å, the energy of this minimum is −1.649 eV, which is slightly higher than that of the linear geometry. When the three atoms separate far away from each other, the image above the contour line is a smooth surface which means the energy of PES is constant.

The characteristics of Fig. 7 are similar to those of Fig. 6. This figure shows the PES with H atom closing on the Li_2 molecule along the angle $\theta = 60.0^\circ$. With the decreasing r value and R value, the energies become lower and lower, and when 2.0 Å < r < 4.5 Å and 0.5 Å < R < 2.0 Å a minimum will be formed, which energy is lower than −1.80 eV. This is not a real three dimensional minimum for this system, we did not get the geometry of the lowest point by optimizing the configuration. From this figure one can make another conclusion that when r is fixed, the change of the energy for PES is slow with an R value larger than 4.0 Å.

Fig. 8 depicts the ground state of the PES for the Li_2H system with $\theta = 90.0^\circ$. From this figure, one can see that when the R is less than 6.0 Å and r is less than 8.0 Å, the electron correlation for this system appeared obviously. And it is clear to see that there is a minimum in this picture. For better analysis of the related features of this minimum, the area near the minimum is amplified and plotted in the lower part of this figure. From this magnified image of this specific area one can see that the energy of this minimum is −2.549 eV, the corresponding r value is 2.53 Å and the R value is 1.17 Å. This minimum is the global minimum for the ground state of the Li_2H system. From analyzing this C_{2v} geometry attachment reaction pathway, one can see that there is no complex for this system.

3.2.2 2D adiabatic PESs of the first excited state. The first excited state PESs for the Li_2H system are displayed in Fig. 9–12 at angles 0.0°, 30.0°, 60.0°, and 90.0°. From these figures one can see that the PESs for the first excited state are more complex than those of the ground state, the details are discussed in the following part. Fig. 9 shows the excited state of PES for Li_2H with an angle fixed at $\theta = 0.0^\circ$. And the important parts are enlarged in plots within the same figure. From the three enlarged plotted panels, one can see that the H atom attacks the Li_2 molecule to form a linear van der Waals minimum (M_4) for the H + Li_2 interaction, with energy 0.195 eV, the value of r is 2.75 Å, and the value of R is 3.90 Å (see panel A). The second complex is enlarged in panel C, this complex is near the products part, the bond distance between the two lithium atoms is 4.45 Å, and the bond distance between Li and H atoms is 1.625 Å, so the geometry of this complex is Li···Li–H, where the energy is 0.145 eV, so this complex can be separate to the product Li + LiH. Between these two complexes there is a transition state TS_1, which has a looser structure, *i.e.*, the bond distance of Li_2 is 3.38 Å and Li–H is 1.95 Å; the energy of this loose structure (0.477 eV) is a little higher than these two complexes, the

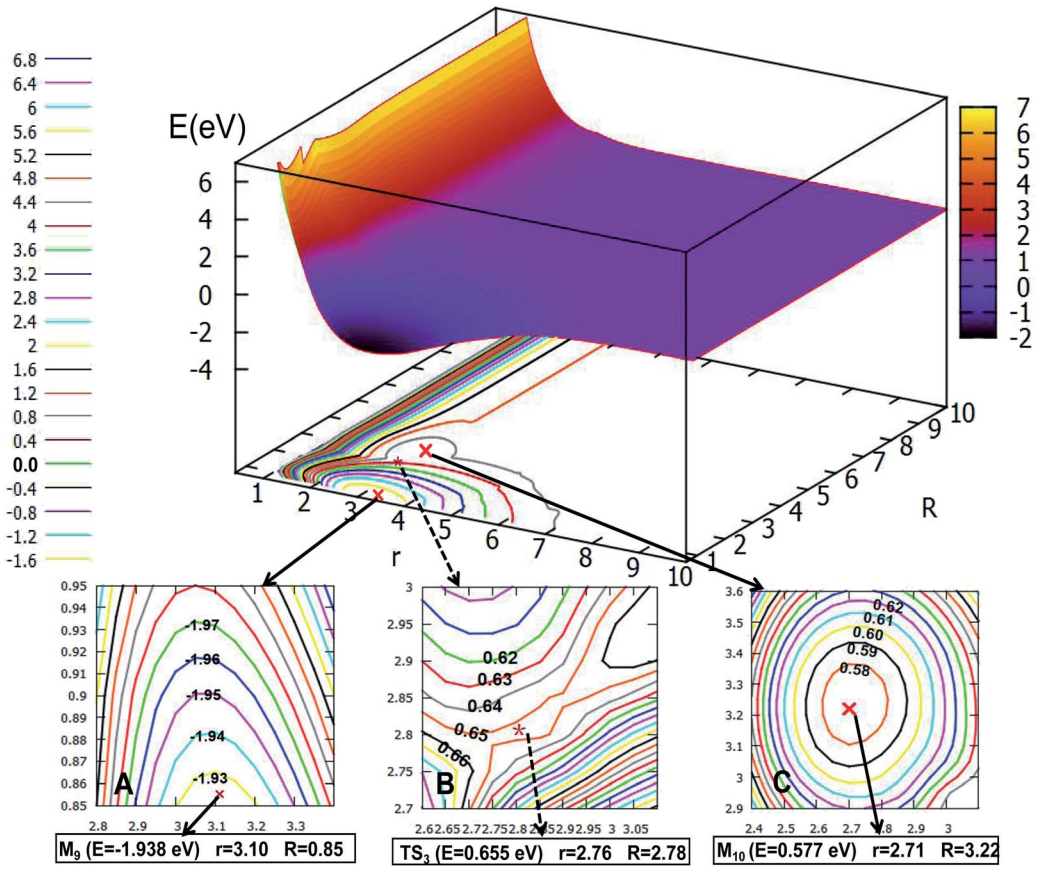

Fig. 12 The first excited state potential energy surface (in eV) for Li_2H and its contour plot as a function of distances r and R (in Å) at angle $\theta = 90.0°$ in Jacobi coordinates. (A) Enlarged plot of the global minimum part M_9; (B) enlarged plot of the transition state part TS_3; (C) enlarged plot of the minimum part M_{10}.

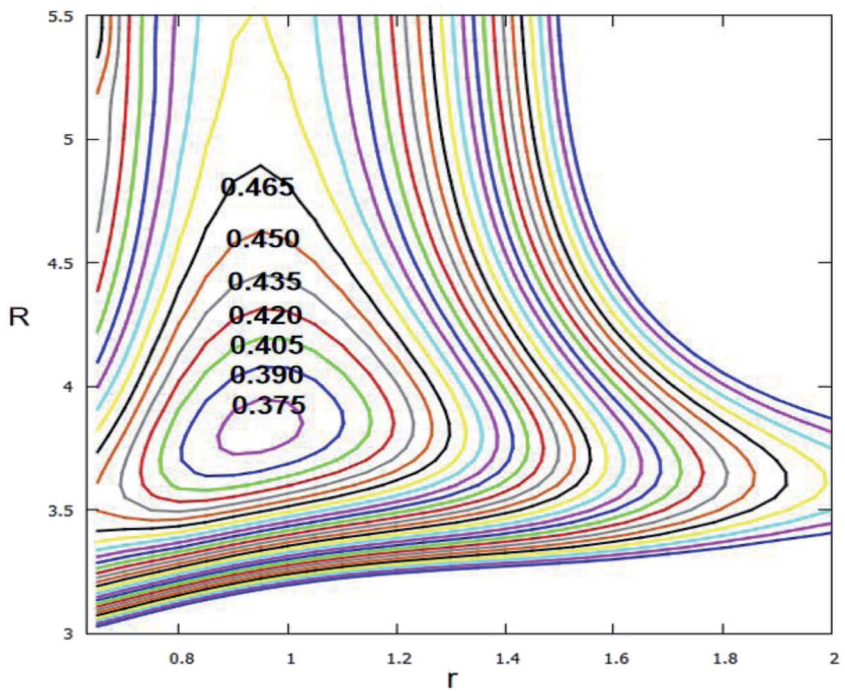

Fig. 13 Avoided crossing point for ground state and the first excited state of the Li_2H system.

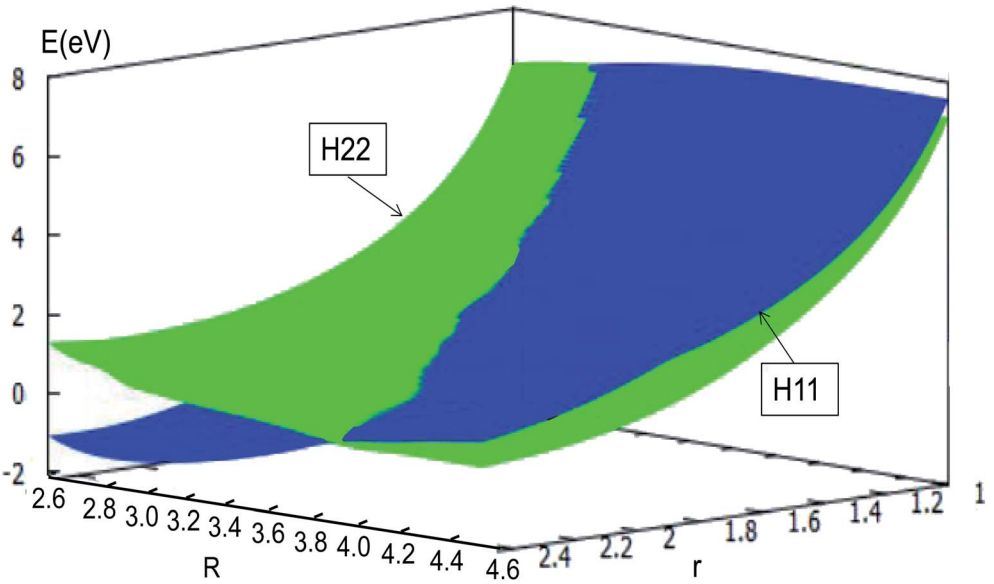

Fig. 14 Diabatic potential energy surfaces (in eV) as a function of distances r and R (in Å) at angle $\theta = 0.0°$ in Jacobi coordinates.

reaction barrier is 0.282 eV, so the reactant complex M_4 easily transforms to the product complex M_5, and *vice versa*.

If the angle is changed to $\theta = 30.0°$, Fig. 10 is obtained. The character of this PES is similar to that of $\theta = 0.0°$; there are two minima and one transition state; the energy of the first minimum (M_6) is 0.268 eV, and the corresponding geometry is $r = 2.78$ Å, and $R = 3.73$ Å; the M_6 overcomes the 0.178 eV energy crossing a transition state (TS_2), whose energy is 0.446 eV, then transforms to another minimum (M_7); the energy of M_7 is 0.078 eV, which is slightly lower than that of M_6, the corresponding structure has r is 2.85 Å and R is 2.98 Å.

When the angle is increased to $\theta = 60.0°$, with decreasing length between H and the Li_2, the minimum M_8, which has an energy of 0.457 eV, will be formed, then the minimum crosses a transition state into another minimum, but these two minima are not real for three dimensional molecules, after optimizing with Gaussian program,[54] these minima will disappear.

The global minimum for the first excited state of Li_2H belongs to the C_{2v} symmetry, the detail of the 2D-PES for the C_{2v} symmetry of this state is shown in Fig. 12. Panel A shows the energy of this minimum (M_9) is −1.938 eV, the corresponding structure has an r value of 3.10 Å and the R value is 0.85 Å. This minimum over 2.59 eV energy (crossing the transition sate TS_3) can reach the second minimum M_{10}. From M_9 to M_{10}, the r value is decreased by 0.39 Å from 3.10 Å to 2.71 Å; and R is extended by 2.37 Å from 0.85 Å to 3.22 Å. The structure of M_9 is

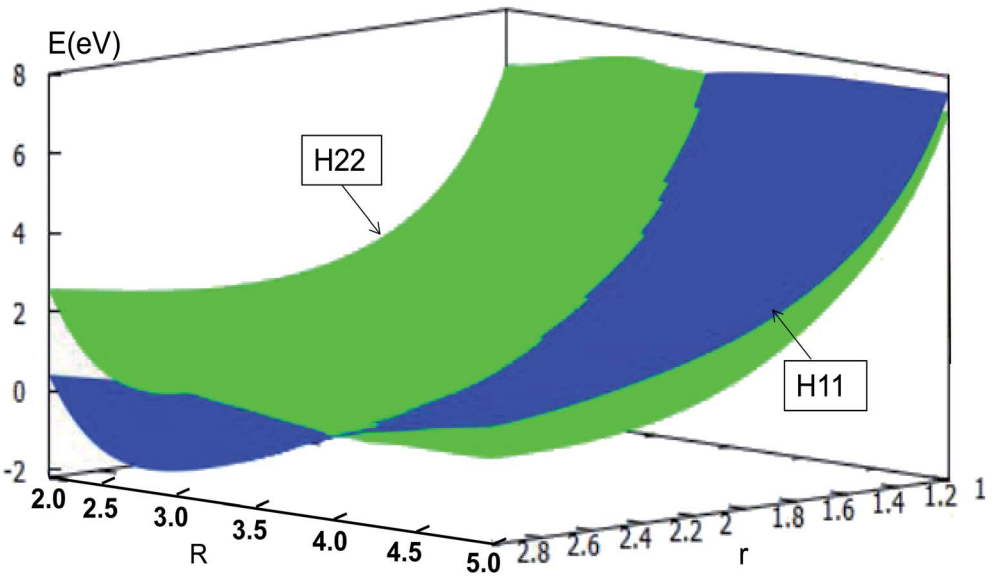

Fig. 15 Diabatic potential energy surfaces (in eV) as a function of distances r and R (in Å) at angle $\theta = 30.0°$ in Jacobi coordinates.

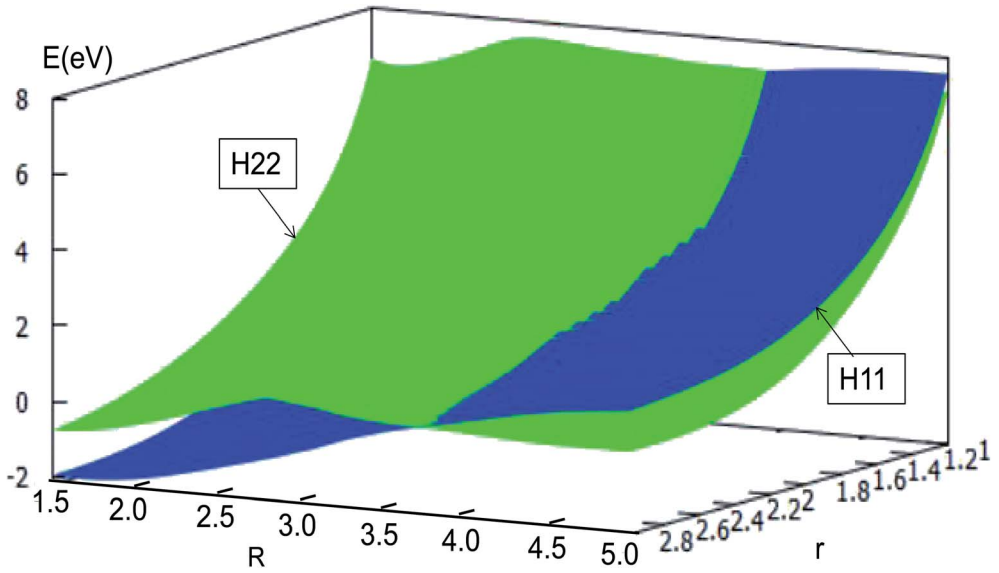

Fig. 16 Diabatic potential energy surfaces (in eV) as a function of distances r and R (in Å) at angle $\theta = 60.0°$ in Jacobi coordinates.

more like that where the hydrogen atom is embedded in the lithium molecule, while M_{10} is more like the hydrogen atom floating away from the lithium molecule.

3.3 Avoided crossing point

The avoided crossing point (ACP) area, is where the consequences of the interaction of an ionic state and a repulsive covalent state, plays an important role in the interpretation of organic phenomena.[55] Since these two states transform each other they only need cross a small energy barrier, and the Born–Oppenheimer rule is not suited to this part. To clearly show the non-adiabatic event between the lowest two adiabatic states of Li_2H, the ACP is studied in this work. Fig. 13 shows the difference in the lowest two adiabatic PESs. From this figure one can see that the minimum energy difference of these two states is approximately 0.369 eV; the structure of this ACP is $r = 0.95$ Å and $R = 3.85$ Å. Since the different energy is so small, the non-adiabatic event happens easily in this range.

3.4 Conical intersection

A conical intersection is a degenerate point of two PESs in the configuration space of a molecule. Because of the strong degeneracy, a nonadiabatic coupling between the two states forms, where the Born–Oppenheimer approximation does not apply. The conical intersection point has been well studied by theoretical scientists.[56–59] The geometry of the conical

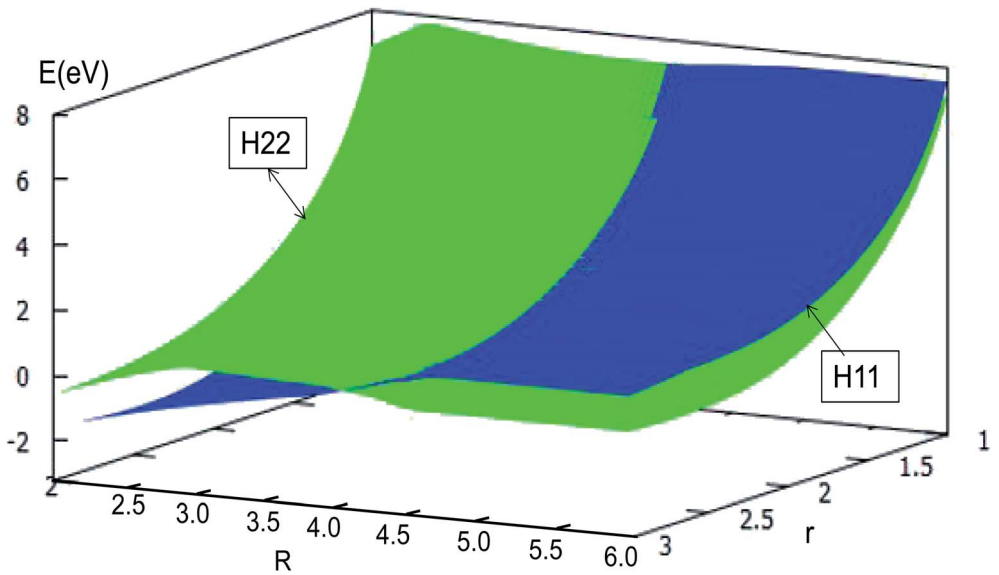

Fig. 17 Diabatic potential energy surfaces (in eV) as a function of distances r and R (in Å) at angle $\theta = 90.0°$ in Jacobi coordinates.

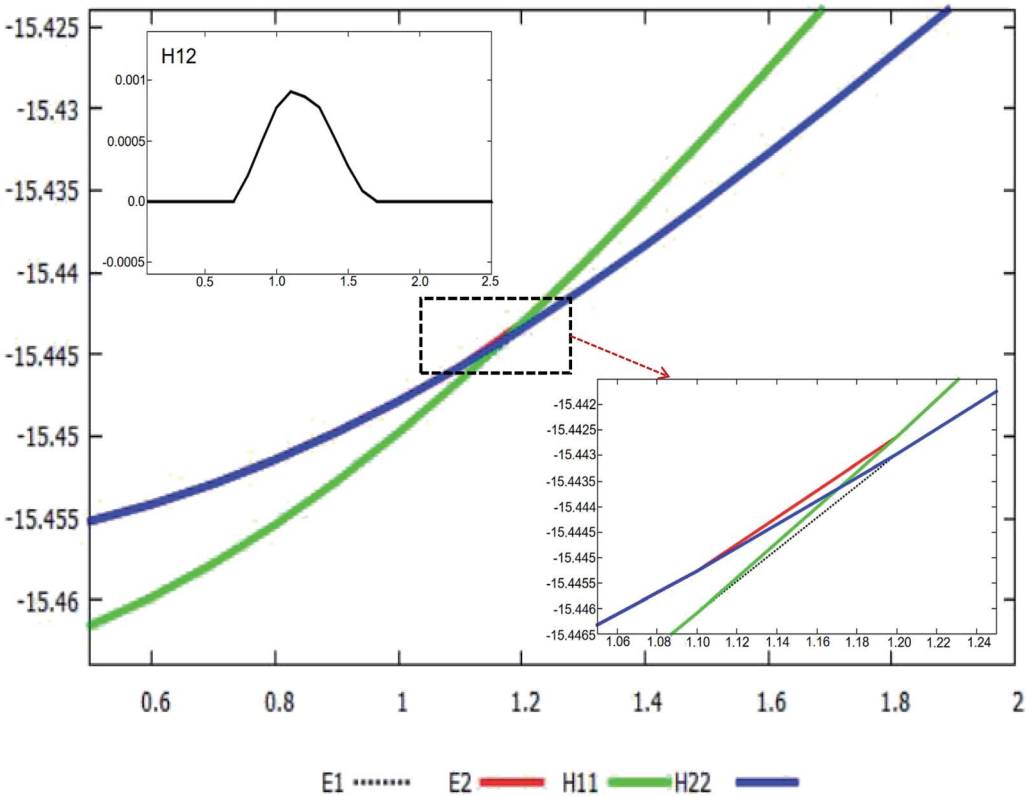

Fig. 18 Cut-out plot of the diabatic potential energy surfaces (in eV) as a function of distance r (in Å), and fixed R at 4.2 Å, at angle $\theta = 90.0°$ in Jacobi coordinates. The crossing part is enlarged and plotted in the bottom panel. The corresponding H_{12} is plotted in the upper panel.

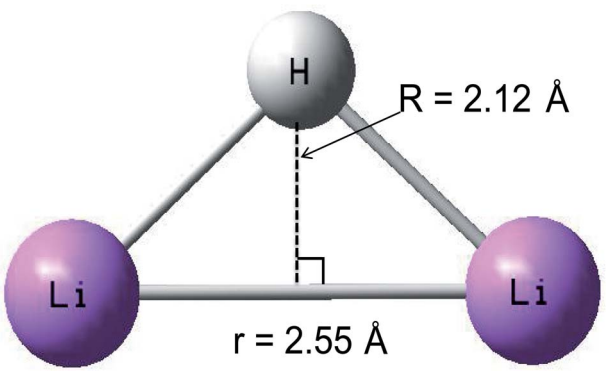

Fig. 19 The conical intersection structure of the Li_2H system.

intersection point is studied in detail, which has C_{2v} symmetry, and the distance of the r is 2.55 Å and the R is 2.12 Å. Combining with Fig. 8, 12 and 19, one can conclude that the geometry of conical intersection point for the title system is between the minimum geometries of the ground state and the first excited state.

3.5 2D diabatic PESs

The adiabatic PESs with different angles and the avoided crossing part of Li_2H system, have been introduced in the above subsections. In order to better understand the phenomena of degeneracy between different adiabatic states in the reaction process, the diabatic PESs are deduced with the adiabatic PESs. Fig. 14–17 describe the two diabatic PESs, H_{11} and H_{22}, with different angles. In these pictures, the blue surface corresponds to H_{11} and the green surface corresponds to H_{22}. From these figures one can analyze that the intersection of H_{11} and H_{22} is in the range of 3.2 Å < R < 3.7 Å, and is almost on the same line; with the decreasing R value, the ground state of the title system has H_{11} potential. *Vice versa* – as the two lithium atoms move away from each other – H_{22} becomes the ground state. For ease of analysis, a section of the crossing part is plotted in Fig. 18, where the R is fixed at 4.2 Å and $\theta = 90.0°$. We could find that the diabatic PESs are very smooth, even near the crossing part. And near the crossing part, the nondiagonal element H_{12} is large, and other parts are zero.

4 Conclusions

The global three dimensional adiabatic PESs for the first two lowest electronic states of Li_2H are deduced with the B-spline fit method, using higher level *ab initio* MCSCF/MRCI energies calculated with V5Z basis sets over a large region of configuration space. In total 74 070 *ab initio* energy points are deduced using two kinds of Jacobi coordinates (reactant coordinate and product coordinate) for each state. The accurate vibrational energies, which for different states of the diatomic molecule of the reactants (Li_2) and products (LiH), are reported for the first

time in the present work: 19 vibrational states are found for the ground state Li_2 molecule; 11 vibrational states and 3 vibrational states are reported for the ground and the first excited states of the product LiH molecule, respectively. The global minima have C_{2v} symmetry and the corresponding relative energies are −2.549 eV and −1.938 eV for the ground state and the first excited state of Li_2H system, respectively; for ease of understanding the non-adiabatic process, the ACP and conical intersection of these two lowest adiabatic PESs are studied in the present work. The study proves that the non-adiabatic reaction event will happen easily since the different energies between these two lowest states is only 0.369 eV. At last, the lowest two diabatic PESs are derived using the adiabatic PESs in the present report.

Conflicts of interest

The authors declare no competing financial interest.

Acknowledgements

This work is supported by the National Natural Science Foundation of China (No. 21573090, 21604031), Jilin Province Science and Technology Development Plan (20150101005JC). This work is supported by the High Performance Computing Center of Jilin University, China.

References

1 D. Galli and F. Palla, *Astron. Astrophys.*, 1998, **335**, 403–420.
2 S. Lepp and J. M. Shull, *Astrophys. J.*, 1984, **280**, 465–469.
3 P. C. Stancil, A. Loeb, M. Zaldarriaga, A. Dalgarno and S. Lepp, *Astrophys. J.*, 2002, **580**, 29–35.
4 V. K. Dubrovich and A. A. Lipovka, *Astron. Astrophys.*, 1995, **296**, 301–306.
5 P. C. Stancil and A. Dalgarno, *Astrophys. J.*, 1997, **479**, 543–546.
6 S. Bovino, M. Wernli and F. A. Gianturco, *Astrophys. J.*, 2009, **699**, 383–387.
7 E. Bodo, F. A. Gianturco and R. Martinazzo, *Phys. Rep.*, 2003, **384**, 85–119.
8 N. J. Clarke, M. Sironi, M. Raimondi, S. Kumar, F. A. Gianturco, E. Buonomo and D. L. Cooper, *Chem. Phys.*, 1998, **233**, 9–27.
9 M. Signore, G. Vedrenne, P. De. Bernardis, V. Dubrovich, P. Encrenaz, R. Maoli, S. Masi, G. Mastrantonio, B. Melchiorri, F. MelchioRRi and P. E. Tanzili, *Astrophys. J., Suppl. Ser.*, 1994, **92**, 535–537.
10 R. Maoli, F. Melchiorri and D. Tosti, *Astrophys. J.*, 1994, **425**, 372–381.
11 P. von Gagué Schleyer and J. A. PoPle, *Chem. Phys. Lett.*, 1986, **129**, 475–480.
12 T. Roy and S. Mahapatra, *J. Chem. Phys.*, 2012, **136**, 174313–174325.
13 W. Wang, Q. Li, Q. Li, X. Yang and G. Le, *Mater. Sci. Technol.*, 2016, **32**, 434–437.
14 P. Gislon and P. P. Prosini, *Int. J. Hydrogen Energy*, 2011, **36**, 240–246.
15 C. H. Wui and H. R. Ihle, *J. Chem. Phys.*, 1977, **66**, 4356.
16 B. Vezin, P. Dugourd, D. Rayane, P. Labastie and M. Broyer, *Chem. Phys. Lett.*, 1993, **202**, 209.
17 R. Antoine, P. Dugourd, D. Rayane, A. R. Allouche, M. AubertFrecon and M. Broyer, *Chem. Phys. Lett.*, 1996, **261**, 670–676.
18 A. L. Companion, *J. Chem. Phys.*, 1968, **48**, 1186–1191.
19 P. Siegbahn and H. F. Schaefer, *J. Chem. Phys.*, 1975, **62**, 3488–3495.
20 C. P. Shukla, N. Sathyamurthy and I. P. Khuller, *J. Chem. Phys.*, 1987, **87**, 3251.
21 S. K. Kim and D. R. Herschbach, *Faraday Discuss. Chem. Soc.*, 1987, **84**, 159–169.
22 S. K. Kim, S. C. Jeoung, A. Lay-Choo Tan and D. R. Herschbach, *J. Chem. Phys.*, 1991, **95**, 3854–3856.
23 W. Fang, X. You and Z. Yin, *Chem. Phys. Lett.*, 1995, **233**, 237–242.
24 Y. Guosen, X. Hui and D. Xie, *Sci. China, Ser. B: Chem.*, 1997, **40**, 342–347.
25 A. M. Maniero, P. H. Acioli, G. M. Silva and R. Gargano, *Chem. Phys. Lett.*, 2010, **490**, 123–126.
26 W. Skomorowski, F. Pawlowski, T. Korona, R. Moszynski, P. S. Zuchowski and J. M. Hutson, *J. Chem. Phys.*, 2011, **134**, 114109–114125.
27 H. V. R. Vila, L. A. Leal, J. B. L. Martins, D. Skouteris, G. M. Silva and R. Gargano, *J. Chem. Phys.*, 2012, **136**, 134319.
28 Y. Z. Song, Y. Q. Li, S. B. Gao and Q. T. Meng, *Eur. Phys. J. D*, 2014, **68**, 3–11.
29 S. B. Gao, J. Zhang, Y. Z. Song and Q. T. Meng, *Eur. Phys. J. D*, 2015, **69**, 111–117.
30 M. L. Yuan, W. T. Li and M. D. Chen, *Int. J. Quantum Chem.*, 2017, **117**, e25380–e25386.
31 Z. L. Zhu, B. Dong and W. Li, *Comput. Theor. Chem.*, 2017, **1115**, 248–252.
32 T. Ferreira da Cunha, H. Vieira Rivera Vila, W. Ferreira da Cunha, L. G. M. de Macedo and R. Gargano, *J. Mol. Model.*, 2017, **23**, 116–126.
33 H. Vieira Rivera Vila, L. A. Ribeiro Jr, L. G. M. de Macedo and R. Gargano, *Sci. Rep.*, 2018, **8**, 1044–1057.
34 T. H. Dunning, *J. Chem. Phys.*, 1989, **90**, 1007–1023.
35 H. J. Werner, P. J. Knowles, G. Knizia, F. R. Manby, M. Schuetz, *et al.*, *MOLPRO, version 2012.1, a package of ab initio programs*, http://www.molpro.net.
36 D. Q. Wang, L. W. Fu, Z. X. Qu, Y. K. Chen and X. R. Huang, *Eur. Phys. J. D*, 2017, **71**, 252–258.
37 L. W. Fu, D. Q. Wang and X. R. Huang, *RSC Adv.*, 2018, **8**, 15595–15602.
38 D. Q. Wang, D. G. Wang, L. W. Fu and X. R. Huang, *Chem. Phys.*, 2019, **517**, 228–236.
39 D. Q. Wang, D. G. Wang, L. W. Fu, J. Y. Wang, G. Shi, Y. C. Li and X. R. Huang, *RSC Adv.*, 2019, **9**, 1929–1932.
40 D. Q. Wang, G. Shi, L. W. Fu, R. L. Yin and Y. B. Ji, *ACS Omega*, 2019, **4**, 12167–12174.
41 R. L. Yin, N. Gao, R. M. Zhang, D. Q. Wang and X. R. Huang, *Chem. Phys.*, 2020, **538**, 110906–110913.

42 N. Sathyamurthy and L. M. Raff, *J. Chem. Phys.*, 1975, **63**, 464–473.
43 M. Patrício and J. L. Santos, *J. Math. Chem.*, 2013, **51**, 1729–1746.
44 R. J. Le Roy, University of Waterloo Chemical Physics Research Report CP-663, 2007.
45 D. Q. Wang, PhD thesis, Siegen University, Germany, 2013.
46 D. He, J. C. Yuan, H. X. Li and M. D. Chen, *Sci. Rep.*, 2016, **6**(1–9), 25083.
47 J. C. Yuan, D. He, S. F. Wang, M. D. Chen and K. L. Han, *Phys. Chem. Chem. Phys.*, 2018, **20**, 6638–6647.
48 A. J. Dobbyn and P. J. Knowles, *Mol. Phys.*, 1997, **91**, 1107–1124.
49 J. N. Byrd, J. A. Montgomery and H. Harvey Michels Jr, *Int. J. Quantum Chem.*, 2009, **109**(13), 3112–3119.
50 J. Kendrick and I. H. Hillier, *Mol. Phys.*, 1977, **33**, 635–640.
51 W. C. Swalley and W. T. Zemke, *J. Phys. Chem. Ref. Data*, 1993, **22**, 87–112.
52 A. M. Maniero and P. H. Acioli, *Int. J. Quantum Chem.*, 2005, **103**, 711–717.
53 C. E. Moore, *Atomic Energy Levels*, National Bureau Standards (U.S.), Cir. No. 467, G. P. O, Washington, DC, 1971, p. 4.
54 M. J. Frisch, G. W. Trucks, H. B. Schlegel, G. E. Scuseria, M. A. Robb, J. R. Cheeseman, G. Scalmani, V. Barone, B. Mennucci, G. A. Petersson, *et al.*, *Revision A. 02*, Gaussian Inc, Wallingford, CT, 2009.
55 L. Salem, C. Leforestier, G. Segal and R. Wetmore, *J. Am. Chem. Soc.*, 1975, **97**, 479–487.
56 M. Baer, *Chem. Phys. Lett.*, 1975, **35**, 112–118.
57 S. Ghosh, S. Mukherjee, B. Mukherjee, S. Mandal, R. Shama, P. Chaudhury and S. Adhikari, *J. Chem. Phys.*, 2017, **147**, 074105–074121.
58 S. Mukherjee, D. Mukhopadhyay and S. Adhikari, *J. Chem. Phys.*, 2014, **141**, 204306–204319.
59 B. Sarkar and S. Adhikan, *J. Chem. Phys.*, 2006, **124**, 074101–074119.